Jour. Fac. Sci., Hokkaido Univ., Ser. VII (Geophysics), Vol. 9, No. 5, 481-508, 1995.

Internal and Meso-γ Scale Structures of Baiu Frontal Rainbands Observed at Shigaraki, Shiga Prefecture by using a Dual-Polarization Doppler Radar

Nobuhiro Takahashi*, Hiroshi Uyeda, Shuji Shimizu, Yoshio Asuma, Katsuhiro Kikuchi, Toshio Harimaya

Department of Geophysics, Faculty of Science, Hokkaido University, Sapporo 060, Japan

Akira Watanabe

Faculty of Education, Fukushima University, Fukushima 960-12, Japan

and

Manabu D. Yamanaka

Radio Atmospheric Science Center, Kyoto University, Uji, Kyoto 611, Japan

(Received November 21, 1994)

Abstract

Baiu frontal convective rainbands were examined by a dual-polarization Doppler radar, MU radar and optical sensor for rain drop size distribution at MU radar site in Shigaraki, Shiga Prefecture, on July 5, 1991. Kinematic analysis revealed that one of the rainbands (rainband A) initiated under a strong horizontal shear, which affected the echo formation with wavelike feature because of shear instability. In this case, a gust front appeared after the formation of the echo ; it changed the propagation direction of rainbands and it contributed for the maintenance of its circulation. The characteristics of the gust front were followings : thickness was less than 1.5 km, propagation speed was 12 ms^{-1}, and the gust front did not apart from the rainband. On the other hand, another rainband (rainband B) which passed over the radar site about 15 minutes after the passage of the rainband A, showed different feature from the rainband A. The gust front did not appear and the echo top height was relatively

* Present affiliation : Communications Research Laboratory, Kashima, Ibaraki Pref., 314.

higher than the rainband A.

Cloud physical analyses were performed to these two rainbands. Estimation of differential reflectivity factor Z_{DR} and horizontally polarized reflectivity Z_H which were obtained by the rain drop size distributions and dual-polarization radar analysis showed good agreement. The rainband A which had relatively lower echo top height (<8 km) with gust front and the rainband B which had relatively higher echo top height (≥ 10 km) without gust front showed distinct differences. The rainband A passed over the radar site during its mature stage, while the rainband B passed over the radar site in its developing stage. Larger rain drops were observed in the rainband A, but smaller rain drops were observed in the rainband B when they passed over the radar site. These differences were assumed to be caused by the passage of different stage of the echoes. Z_{DR} distributions expressed that the earlier stage of both rainbands showed relatively smaller Z_{DR} and smaller variability of Z_{DR} than their mature stage. In addition, the rainband A which was formed below 6 km (0°C level was 4.5 km in height); this suggests that the raindrops in this rainband was formed under warm rain process. On the other hand, the rainband B which was formed above 8 km in height suggests cold rain process. It was thought therefore that the environmental condition of the Baiu season, which was neutral or slight unstable structure below 6 km with stable layer above it and almost saturated condition below 6 km, might influence the development processes of the rainbands.

1. Introduction

In the Baiu season (rainy season of Japan), several types of rainfall events occur along the Baiu front that is expressed as steep gradient of low level water vapor. One of them is a long lasting weak rainfall, which is produced by stratiform cloud. This type of rainfall mainly characterizes the Baiu frontal rainfall. On the other hand, especially at the late period of the Baiu season, convective severe storms develop on the western part of Japan associated with cloud clusters along the Baiu front. Convective clouds with heavy rainfall are often generated under the condition of moist and slightly unstable atmospheric structure. Heavy rainfall events during the Baiu season are mainly caused by these convective clouds which have relatively small scale (meso-β scale).

Historically, an importance of mesoscale (meso-α scale) for the Baiu frontal heavy rainfall was pointed out by Ninomiya and Akiyama (1972, 1973) and Akiyama (1978) who named the scale as "medium scale". Akiyama (1984a, b) analyzed conventional radar images to describe organization process of convective cloud. In her result, highly organized convective clouds (cloud clusters) are consisted by several convective clouds and are maintained by merging of newly developed convective clouds. Ogura et al. (1985) clearly described the organization processes in the case of Nagasaki heavy rainfall event in 1982 from the viewpoint of meso-β scale phenomena. They also reported the existence of strong convective outflow (wind gust) associated with

the convective clouds. On the meso-γ scale phenomena, recent studies such as Westcott and Kennedy (1989) and Tao and Simpson (1989) reported that the merging effect among convective clouds is important for cloud organization and convective outflow played an important role for the organization. Studies on the meso-γ scale characteristics of the Baiu frontal rainband were not so many, because of insufficient observations by high resolution remote sensing facility such as Doppler radars.

In this study, a kinematic analysis of convective clouds observed between 02JST and 04JST on July 5, 1991, which appeared as two narrow rainbands at the leading edge of the mesoscale precipitation system, was performed using an X-band Doppler radar and VHF Doppler radar, MU radar (Middle Upper radar of Kyoto University ; e.g., Fukao et al., 1988), at the MU radar site in Shigaraki, Shiga Prefecture.

In addition to the kinematic analysis, results of cloud physical observation using dual-polarization radar and rain drop size distribution derived from optical sensor are presented. The cloud physical mechanism is also important to characterize the Baiu frontal rainfall events. Because, under the mid-latitudinal wind field, the atmospheric condition of the Baiu season is quite different from the ordinary extra-tropical frontal systems such as warm and cold fronts, rather similar to the tropics which has warm and moist atmosphere, the cloud physical processes may be different from both frontal system and tropical clouds. In this study, the Z_{DR} (differential reflectivity factor) was analyzed carefully as a measure of cloud physical characteristics to express the Baiu frontal rainband.

2. Method

Figure 1 shows the observation area of this case with the radar observation range (60 km). The dual-polarization Doppler radar provides Doppler mode with 60 km observation range and dual-polarization mode, that was mainly utilized in RHI scan, with 30 km observation range (hereafter Doppler radar means Doppler mode and dual-polarization radar means dual-polarization mode). The specification of the radar is shown in Table 1. The Doppler radar obtains reflectivity, Doppler velocity, and spectrum width of Doppler velocity with a resolution of 250 m in range, 0.7° in azimuth (PPI) and 0.25° in elevation (RHI). The dual-polarization radar obtains the raw data of horizontally polarized reflectivity (Z_H) and vertically polarized reflectivity (Z_V) pulse to pulse (alternately) with a resolution of 125 m in range and 0.05° in elevation. Polar-

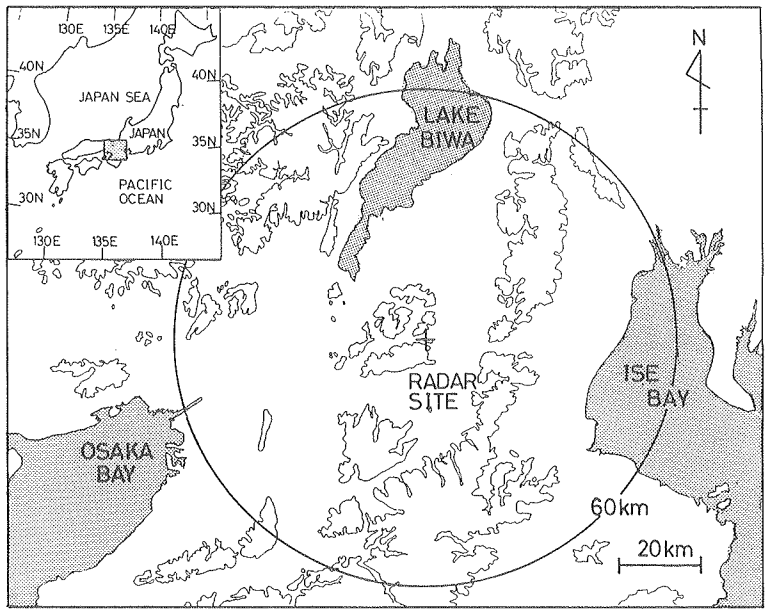

Fig. 1. Topographical map of the observation area with 200 m contour lines. The location of the Hokkaido University Doppler radar and its 60 km range is depicted as a cross and a circle, respectively.

Table 1. Specification of the dual-polarization Doppler radar.

Hokkaido University Dual-Polarization Doppler Radar		
Parameter	Dual-Polarization	Doppler
Wave length (cm)	3.2	3.2
Maximum range (km)	31.5	63.5
Nyquist velocity (m/s)		±12.0
Pulse duration	0.8	0.4
Pulse repetition frequency (Hz)	750	1,500
Azimuthal resolution (deg.)	0.35	0.7
Beam width (deg.)	2.0	2.0
Number of samples	252	254
Gate spacing (m)	62.5	62.5
Sample spacing (m)	125	250
Antenna rotation (rpm)		1
Antenna diameter (m)	1.2	1.2

imetric parameter of Z_{DR} is defined as

$$Z_{DR}=10 \log (Z_H/Z_V). \quad (1)$$

The value Z_{DR} generally represents the characteristics of drop size distribution of rain; a large Z_{DR} means a rainfall consisted of relatively large drops, and a small Z_{DR} means a rainfall consisted of relatively small drops. Detailed explanation of Z_{DR} will be described in section 5. During this observation, the dual-polarization Doppler radar located at the MU radar site. Observations were made at 15 minute intervals mainly using Doppler mode scan and dual-polarization mode was operated intermittently. The PPI scans were set at a relatively high elevation angle; this was necessary because the main purpose of this observation was to compare MU radar wind profiles to Doppler weather radar wind profiles (Shimizu et al., 1992) and the topography around the radar site (Fig. 1) prevents low elevation observation.

In addition to the dual-polarization Doppler radar data, MU radar data, six hourly sounding data, surface meteorological data (pressure, temperature, and wind speed and direction), rain drop size distributions by an optical sensor, and vertical pointing radars (C-band and Ku-band) at the radar site were available for analysis. Vertical profiles of u, v, and w components of wind were obtained by MU radar about 10 minute intervals with vertical resolution of 300 m above 1.5 km in height. The specification of MU radar is presented by Fukao et al. (1988).

3. Environmental condition

Figure 2 shows surface weather charts of 21JST (Japan Standard Time: JST=UTC+9 hours) on July 4 and of 09JST on July 5 in order to depict the synoptic conditions of this case (rainbands were observed between these two times: from 02JST to 04JST). At 21JST on July 4, the Baiu front was located over the middle of Japan, associating with low pressure system, and stretching from northwest to southeast over the observation area (the observation area is indicated by a circle). At that time, a weak rainfall was observed at the radar site and stratiform echo was observed by the Doppler radar. At 09JST on July 5, the low pressure system moved eastward and the Baiu front changed its form to warm and cold fronts. The cold front located south of the radar site. This transition of the front indicated that the rainband initiated when the front propagated over the radar observation area and the front had a characteristic such as a cold front (represented by cold air advection) over radar observation

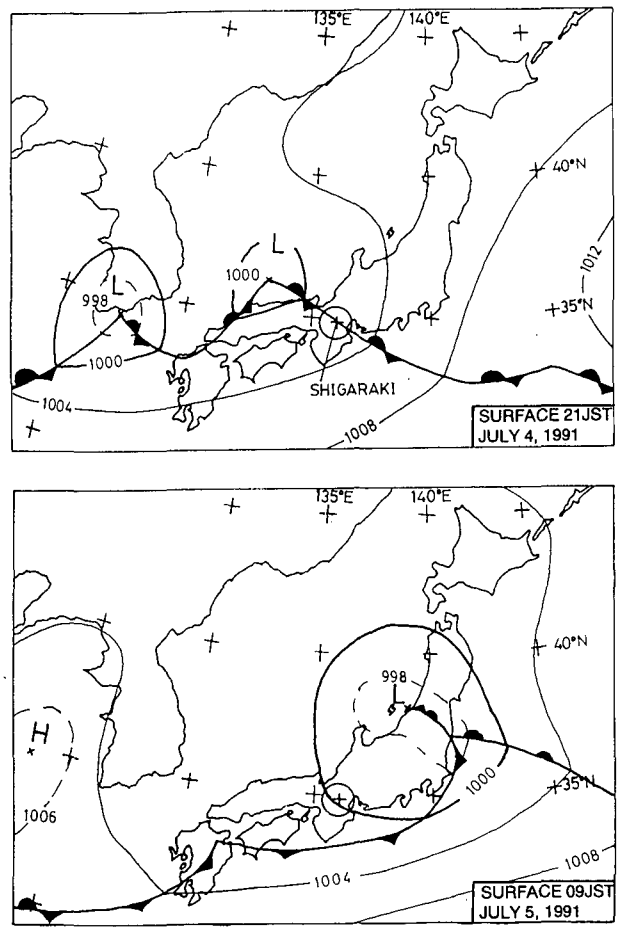

Fig. 2. Surface weather charts at 21JST on July 4 and at 09JST on July 5, 1991. The location of the radar site and its 60 km range is depicted as a cross and a circle, respectively.

site. Successive sounding data at the radar site indicated low level (below 4 km) cold air advection appeared after passing the rainband (between 03JST to 09JST). Upper level cold air advection, however, appeared one day after this case (July 6).

Vertical profiles of potential temperature (θ), equivalent potential temperature (θ_e), and saturated equivalent potential temperature (θ_e^*) at 03JST (the balloon was launched from the radar site just before the passage of the rainbands) on July 5 (Fig. 3) show a saturated condition with slight convectively

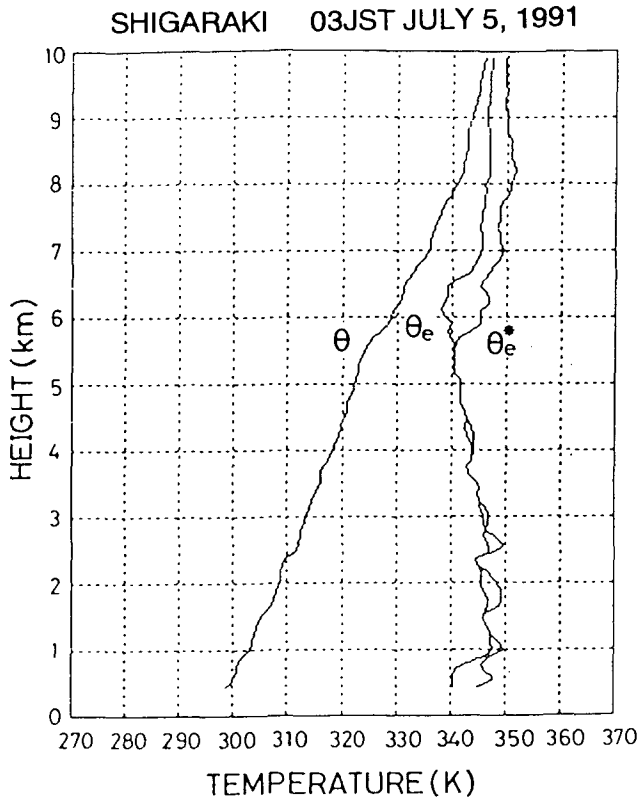

Fig. 3. Verical profiles of potential temperature (θ), equivalent potential temperature (θ_e), and saturated equivalent potential temperature (θ_e^*) at 03JST (The sonde was launched at the radar site just before the passage of the rainband) on July 5, 1991.

unstable below 5.5 km in height and stable layer existed above it. Because of a weak rainfall from a stratiform echo began several hours before the rainband passage, the atmospheric condition was neutral stability and almost saturated. It is typical condition during the Baiu season.

Time series of wind profiles derived from MU radar are shown in Fig. 4. Before the passage of rainbands (first passage is indicated by the arrow), a strong southwesterly wind ranged from 25 ms^{-1} to 35 ms^{-1} dominated below 8 km in height. During the passage of rainbands (0330 to 0340JST), a relatively disturbed westerly wind appeared below 6 km. After the passage of rainbands, the wind field returned almost the same condition as existed before passage ; the only difference was that southwesterly wind speed had dropped to between 25

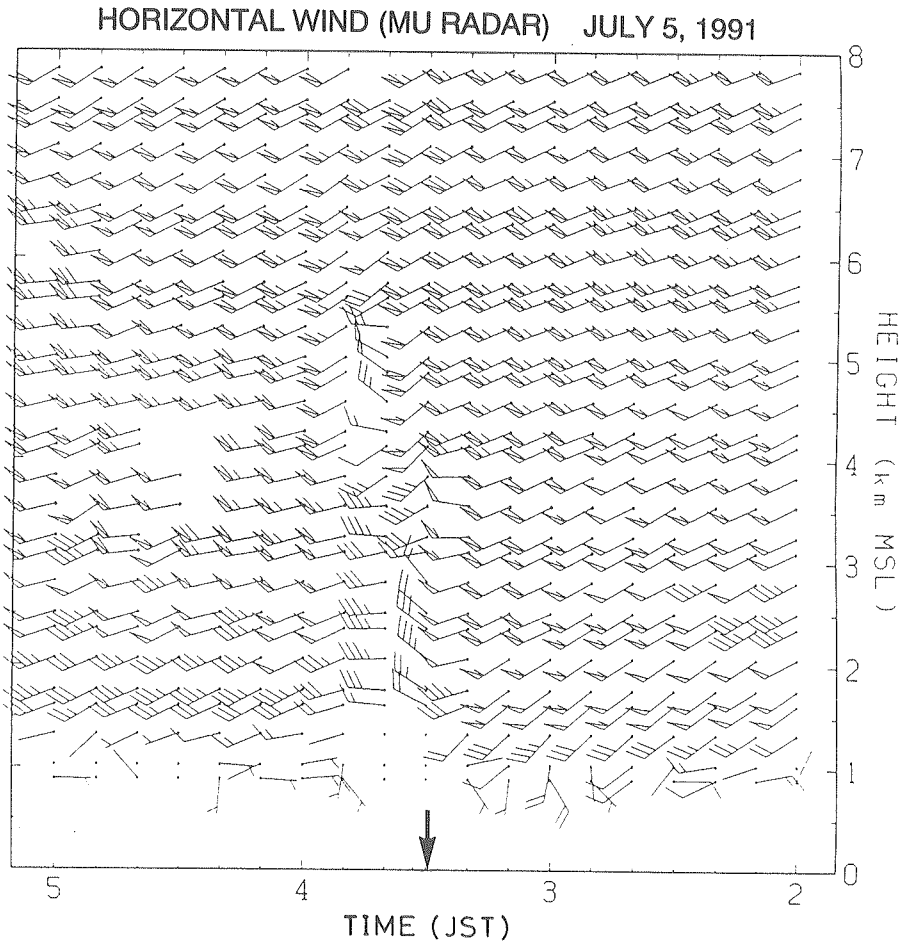

Fig. 4. Wind profiles from 02JST to 05JST on July 5, 1991, obtained by MU radar data. Full barb is a wind speed of 5 ms^{-1}, half barb is of 2.5 ms^{-1}, and pennant expresses that of 25 ms^{-1}.

ms^{-1} and 17.5 ms^{-1} below 3 km in height.

4. Doppler radar observation of the rainbands

Figure 5 shows the distribution of radar echoes taken by JMA (Japan Meteorological Agency) Osaka radar around MU radar site at 0337JST on July 5. This figure indicates that a mesoscale system located northwest of the Doppler radar site, and intense rainband located at the leading edge of the

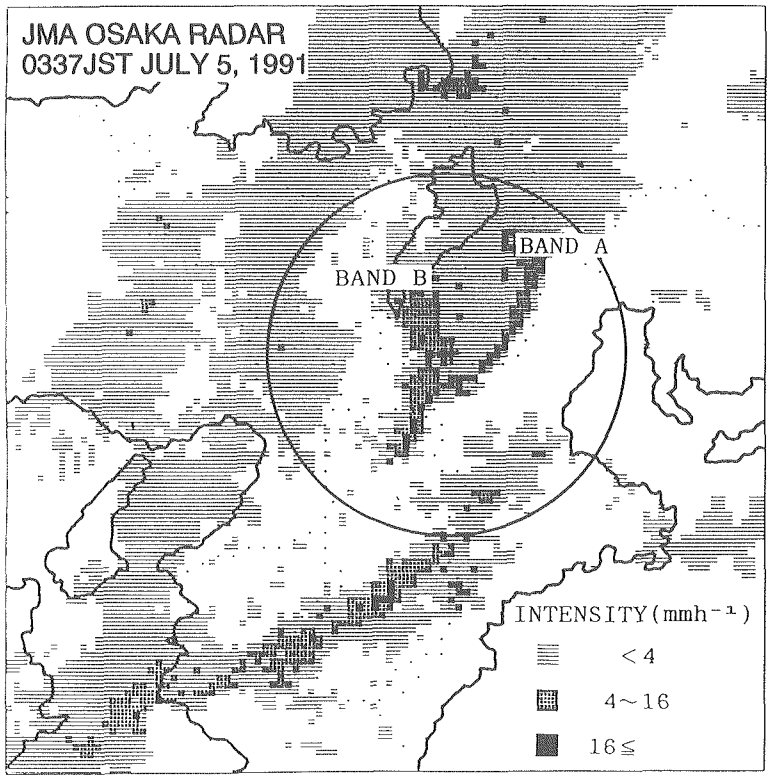

Fig. 5. JMA Osaka radar image around MU radar site at 0337JST on July 5, 1991.

system. As shown in Fig. 5, two intense rainbands (A and B) existed within the Doppler radar observation range. These rainbands passed over the MU radar site. Transition of the rainbands is shown in Fig. 6 from the JMA radar (Osaka radar) data. From 0200JST to 0245JST, a rainband existed west of the MU radar site, and this echo split into two rainbands of A and B or might collapse and generate new two rainbands between 0300JST and 0330JST. Both rainbands moved to the east and extended its area from northeast to southwest.

Figure 7 shows a detailed structure of foregoing rainband A in Fig. 6, from 0236JST to 0335JST that was detected by the Doppler radar. The rainband A was first observed within the Doppler radar observation area at 0236JST. The rainband propagated east at a speed of about 20 ms^{-1}. As shown in JMA Osaka radar data, this rainband was formed at around 0230JST and moved eastward. This rainband was consisted of several echo cells. The propagation direction

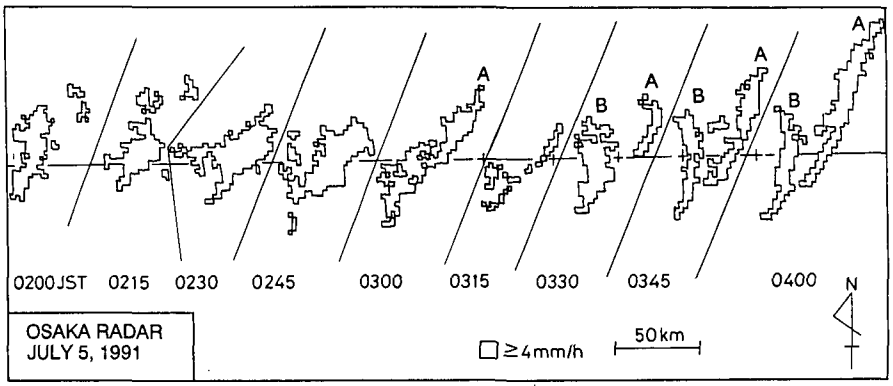

Fig. 6. Time series of intense area (>4 mm h^{-1}) of rainbands from 02JST to 04JST on July 5, 1991. The location of the Doppler radar site relative to the echo from 03JST to 04JST was indicated by (+). The rainband A is indicated by 'A' and the rainband B is indicated by 'B'.

of rainband drastically changed to southeastward between 0251JST and 0307JST (which was not detected by JMA Osaka radar), moved with a speed of about 12 ms^{-1} and changing its shape to a narrow rainband. The changes in propagation direction and the structure of rainband are explained by low altitude wind field, which was calculated by the sector VAD (Velocity Azimuth Display; see Browning and Wexler, 1968) method and is shown in Fig. 8. The principle of the sector VAD method is followings; the VAD method can calculated wind field by assuming the linearity of the wind within the observation range, but it can not be applied to the cases where discontinuity exists within the area. Then the sector VAD method is possible to calculate a wind for a limited area of low elevation PPI data. In this study, a wind field was calculated within a fan-shaped area of 60° in azimuth and 2 km in range from PPI data with 4° elevation angle. Before the formation of the narrow rainband (0251JST, top frame in Fig. 8), the prevailing wind (southwesterly) dominated in and around the rainband. As in Fig. 4, a stronger southwesterly wind dominated over the radar site (at the south of the rainband, it coincides with the wind profile observed before the passage of rainband over the MU radar site in Fig. 4); on the other hand, relatively weak wind existed behind the rainband (see the wind profile observed after the passage of rainband in Fig. 4).

A large horizontal shear was considered to influence the echo formation, especially an echo cell interval because of the shear instability, which was pointed out by Hobbs and Persson (1982), Mueller and Carbone (1987), and

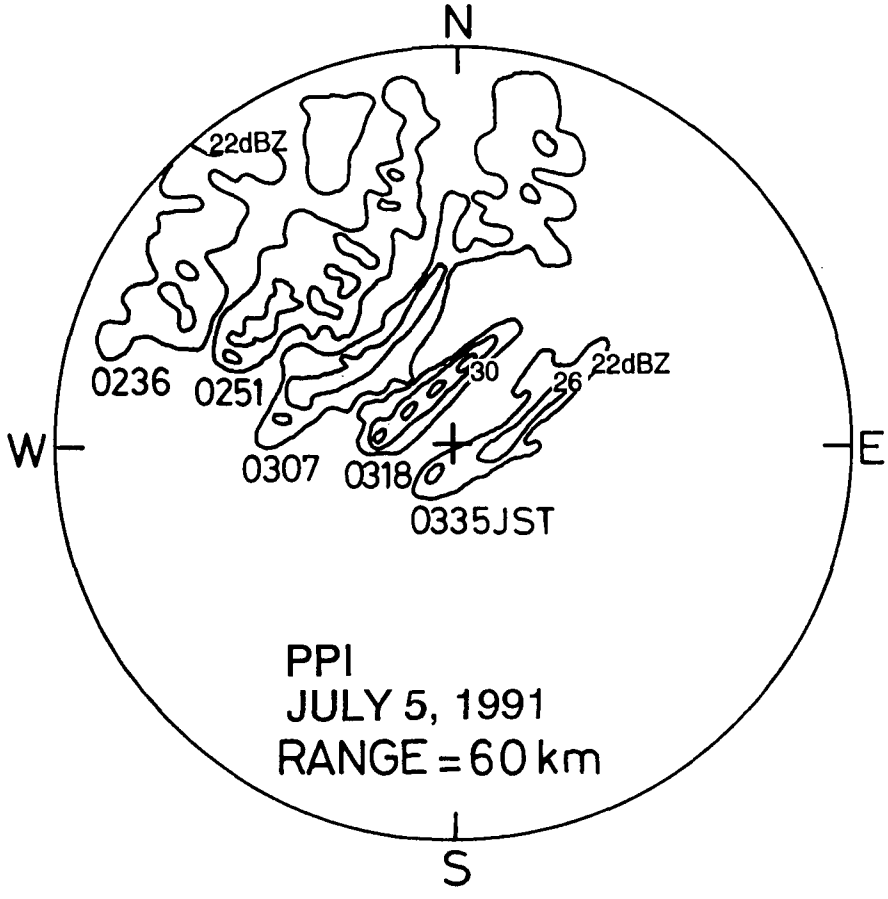

Fig. 7. Transition of PPI scan radar echoes (elevation=4°) from 0236JST to 0335JST on July 5, 1991. Contour interval is 4 dBZ from 22 dBZ.

Lemaitre and Brovelli (1990) on the cases of cold frontal rainbands. A strong northwesterly wind appeared at 0308JST in the lower left side in the bottom frame in Fig. 8, while southwesterly wind remained in front of the rainband. A strong convergence was generated on the frontal part of the rainband. This southwesterly wind forced the rainband to propagate southeastward. This rainband passed over the radar site at 0326JST, causing intense rainfall (rainfall intensity was about 60 mmh^{-1} from 2 minute data).

The vertical structure of this rainband was examined using RHI data. At the earlier stage around the appearance time of the rainband A within the observation area, the rainband had echo top height about 10 km as shown in Fig.

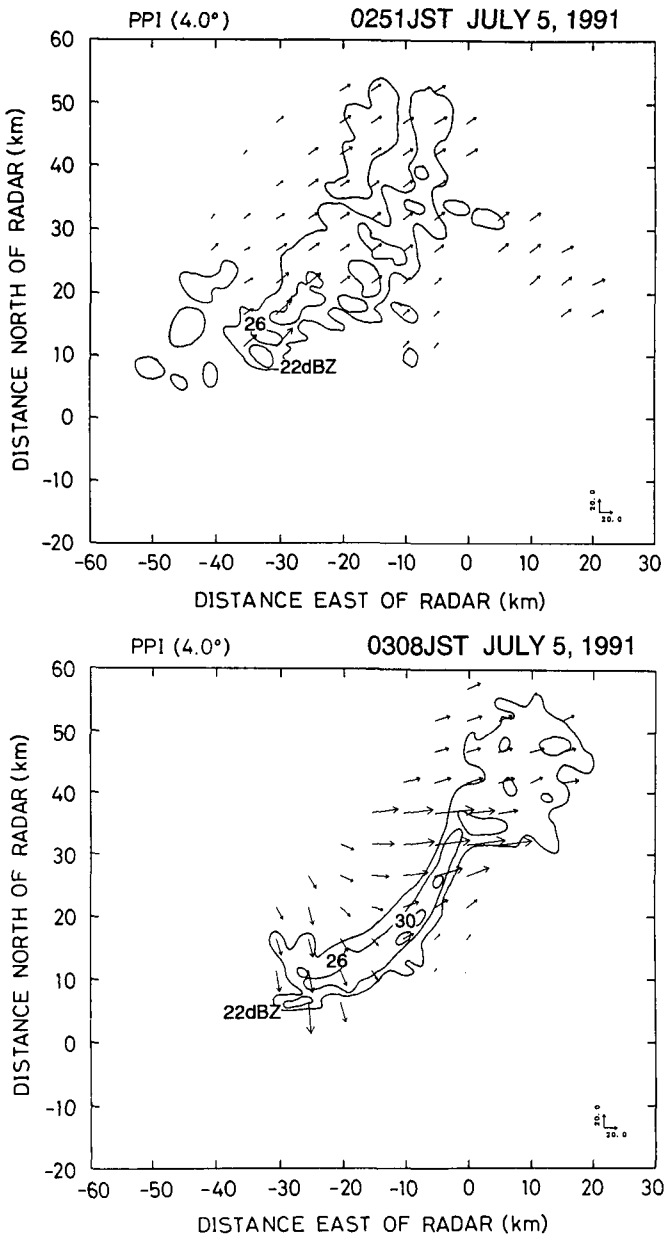

Fig. 8. PPI scan radar echoes (elevation=4°) at 0251JST and 0308JST on July, 5, 1991, with wind fields which were calculated by sector VAD method. Contour interval is 4 dBZ from 22 dBZ.

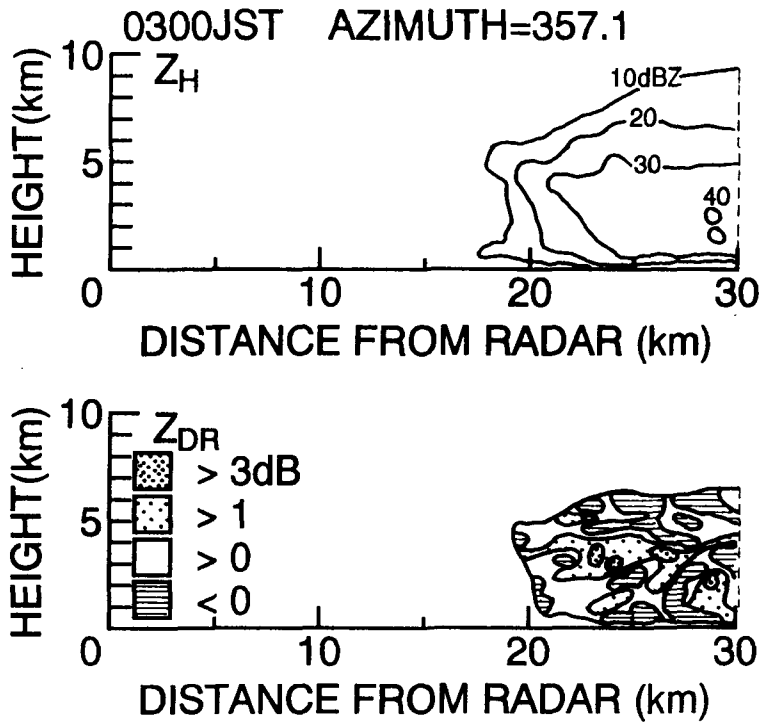

Fig. 9. Vertical cross section (RHI) of the rainband A at the azimuth of 357.1° at 03JST on July 5, 1991. Top: Reflectivity (Z_H) in dBZ. Contour interval is 10 dBZ from 10 dBZ. Bottom: Differential reflectivity factor (Z_{DR}) in dB.

9. As mentioned in Figs. 7 and 8, the rainband propagated to the east at this time. About 13 minutes later from the time of Fig. 9, the structure of the rainband changed, and the echo top height at the strong echo region became lower, less than 6 km. Also, the top frame of Fig. 10 shows two dimensional wind fields that were calculated by using Doppler velocity data. A strong updraft appears at the front of the rainband around 13 km from the radar site and a downdraft appears just behind the area of strong reflectivity. This downdraft caused the low altitude gust, which is shown in Fig. 10, and enhanced the updraft. It is closely related to the changes of horizontal wind field and propagation direction.

Figure 11 shows a surface meteorological observation data in which a gust was detected at the radar site having a north-northwesterly wind with a speed of 11 ms^{-1}, and accompanied by a pressure rise of 2 hPa and a temperature drop

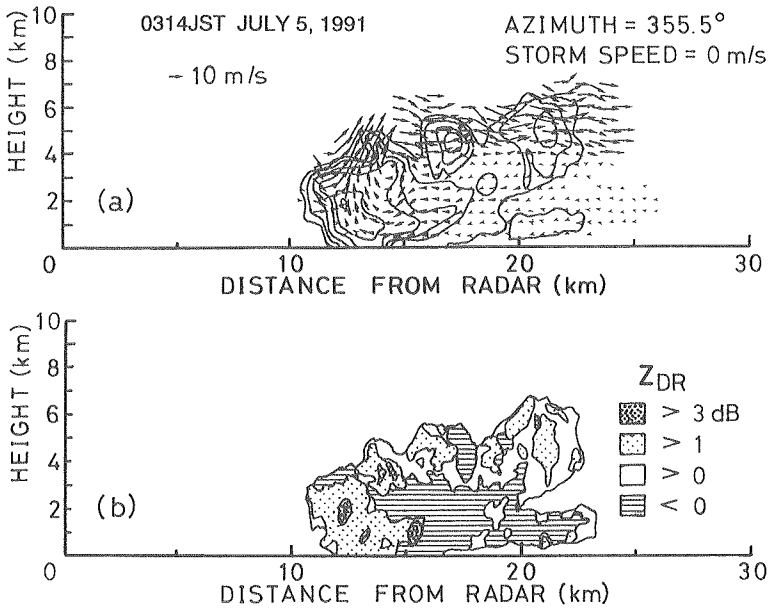

Fig. 10. Vertical cross section (RHI) of the rainband at the azimuth of 355.5° at 0314JST on July 5, 1991. Top: Reflectivity with two dimensional wind field which was calculated by using RHI scan Doppler velocity data at 0314JST on July 5, 1991. Contour interval is 4 dBZ from 22 dBZ. Bottom: Differential reflectivity factor (Z_{DR}) in dB.

of 1.5°C. This north-northwesterly wind continued for about 40 minutes. Since the long lasting north-northwesterly wind did not appear in the MU radar observation data in Fig. 4 at the times other than 0330JST and 0340JST, the thickness of this gust was at least less than 1.5 km because of the MU radar wind data was available higher than 1.5 km in height.

This case study expressed that the echo formation of the rainband A was caused by strong horizontal shear, as shown in Figs. 4 and 8. The echo moved eastward firstly and the propagation direction of the rainband was forced to the southeast after the appearance of the gust front (convective outflow). The initiation of the gust front is not clear from the Doppler radar data alone. It is assumed however that a well-developed rainband collapsed as indicated in Fig. 5, and produced an outflow. The outflow as a gust front generated a new rainband in front of it and changed its propagation direction to the southeast. This assumption was supported by the surface rainfall distribution, derived from AMeDAS, as shown in Fig. 12. From 03JST to 04JST, a strong rainfall was

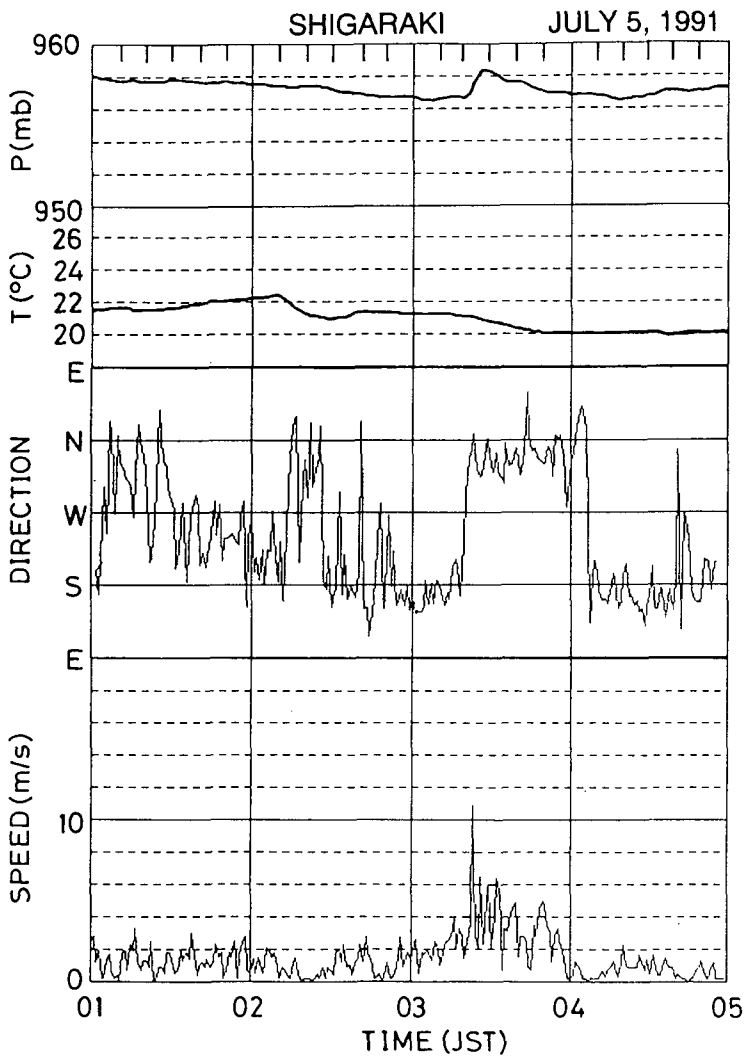

Fig. 11. Surface meteorological observations of transitions in pressure, temperature, and wind from 01JST to 05JST on July 5, 1991, at the radar site.

observed western portion of the radar observation area. From JMA Osaka radar in Fig. 5, the heavy rainfall area (>20 mm) coincided with echoes between 0300JST and 0345JST, especially the rainfall of the western portion was brought around 0300JST. The heavy rainfall area did not appear before and after this period around this area during this event. This indicates that a well-developed

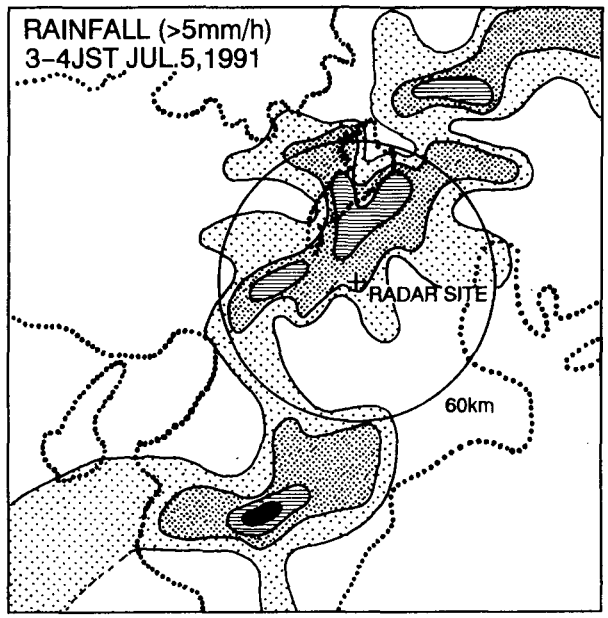

Fig. 12. Distribution of surface rainfall amount from 03JST to 04JST derived from AMeDAS network. Light stippled area expresses rainfall >5 mm, heavy stippled area expresses >10 mm, shaded area expresses >20 mm, and >40 mm area is shaded black. Dotted line indicates the coastal line.

convective cloud brought heavy rainfall during a mature or dissipating stage. The formation and developing processes are schematically illustrated in Fig. 13. In the earlier time (0240JST), the rainband developed under the conditions of strong horizontal shear at low altitudes. About 15 minutes after the echo was formed, a gust front appeared in the rainband although it couldn't be distinguished whether it was produced by the collapse of a preexisting rainband or not. After that, the gust front contributed to change the structure of the rainband and to change the propagation direction of the rainband.

For the gust front in this case, the depth, propagation speed, and occurrence mechanism are summarized as follows. Firstly, the depth of the gust is deduced to have been less than 1.5 km, because the gust wind appeared only in the surface wind field, which was not detected by the MU radar. Furthermore, as shown in Fig. 8, PPI data with 4° elevation angle showed the gust wind component. This result indicates that the gust existed at a height lower than 1.5 km. Secondly, as mentioned before, the gust front propagation speed was about 12 ms^{-1} as calculated by the echo movement and surface gusting wind. Lastly, the JMA

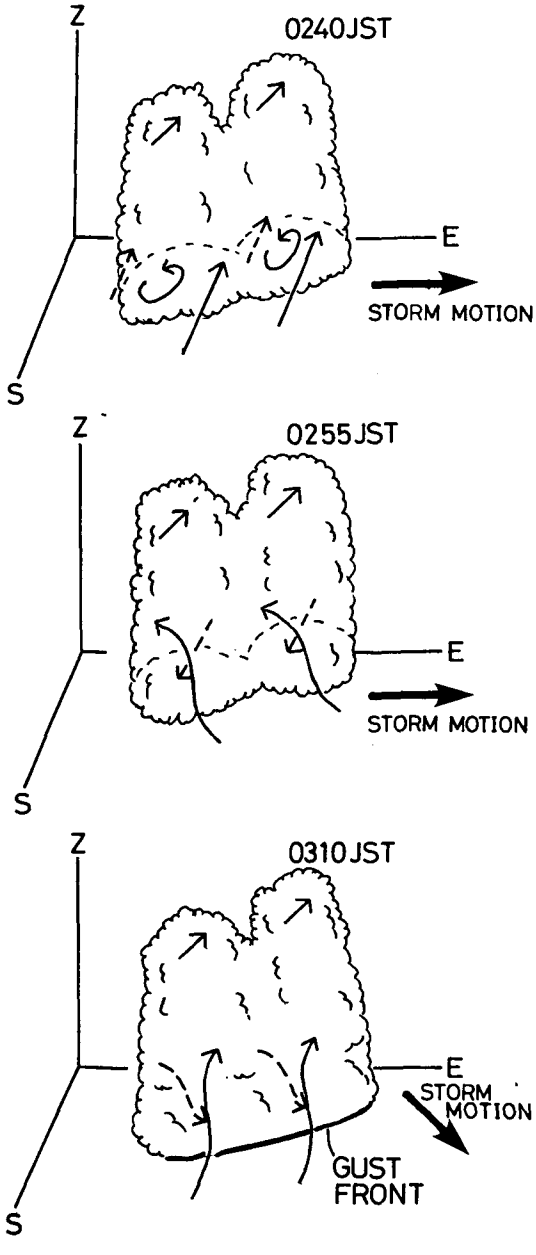

Fig. 13. Schematic illustrations of the radar echo evolution process of the rainband A. Arrows express the flow front of the rainband (solid) and rear of the rainband (dashed).

Osaka radar data analysis (Fig. 5) suggests that the occurrence mechanism of the gust front (convective outflow) was brought by the collapsing of a well-developed echo. The gust front changed the structure and propagation direction of the rainband that existed in front of the gust producing echo.

Major features of this gust front are similar to the cases of the Baiu frontal rainband in Kyushu (Takahashi, 1994) in which gust front located just ahead of the rainband and propagated almost same speed of rainband; also, this gust front enhanced the low level convergence of the rainband that was generated under a condition of frontal instability. The differences between this case and the cases in Kyushu from the view point of the stability of the atmosphere, wind profiles, and front stationariness were followings; In this case, the rainband developed in neutrally stratified condition, larger scale forcing of the front played an important role for the development of the rainband. This feature was similar to a Mei-yu frontal rainband described by Ray et al. (1991) and Lin et al. (1992). On the other hand, both unstable condition and the larger scale forcing were important for the cases of Kyushu. Wind speed in this case was much stronger than that observed in Kyushu during the late period of the Baiu season. Also, in this case the front was similar to a cold front, while in the cases of Kyushu, the Baiu front was stationary. This feature is also similar to the tropical gust fronts which were observed at Manus Island, Papua New Guinea (Takahashi and Uyeda, 1995).

About 15 minutes after the passage of the rainband A, the rainband B passed over the radar site. Because the rainband approached from west of the radar site, the rainband was not detected by the Doppler radar due to mountains which located at the west of the radar. When the rainband B passed over the radar site, the surface meteorological elements indicated that no specific change occurred associating with the passage (see Fig. 11). The maximum rainfall intensity in 2 minutes was 92 mmh^{-1}; this was larger than the rainfall intensity of the rainband A. Just after passing the rainband B, the radar observation was unfortunately interrupted at 0342JST due to stoppage of electric power supply because of lightning discharge from the rainband. It also indicated the active convection dominated in the rainband. Since the radar system restored around 0350JST, we only obtained the Doppler radar data after 0350JST on rainband B and just before the passage of the rainband. At 0350JST, the rainband moved to the east of the radar site with the propagation speed of 20 ms^{-1}.

The transition of the vertical structure of the rainband B was not clear before passing over the radar site. Figure 14 shows that the vertical structure of rainband B just before passing over the radar site. From this figure, the echo

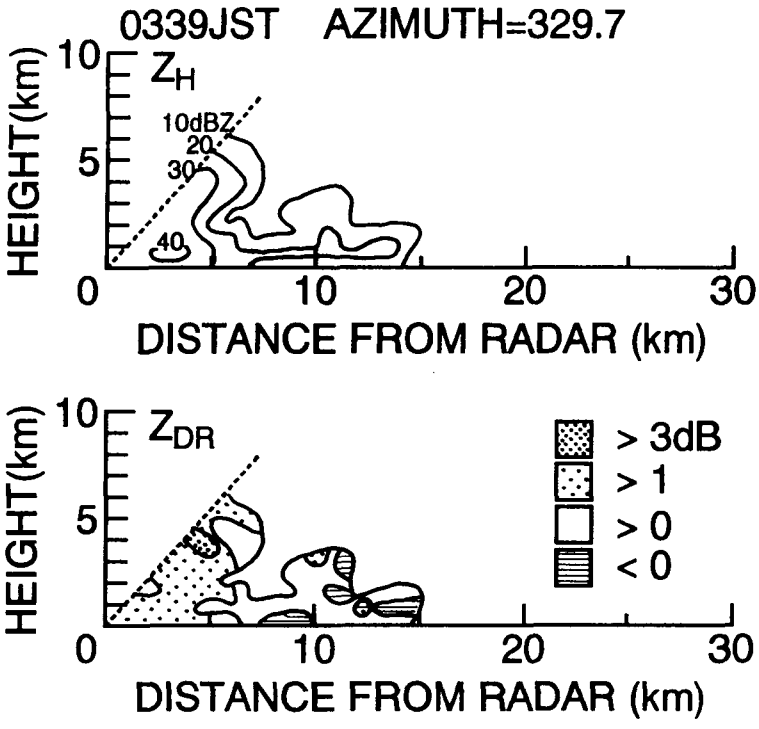

Fig. 14. Vertical cross section (RHI) of the rainband A at the azimuth of 329.7° at 0339JST on July 5, 1991. Top: Reflectivity (Z_H) in dBZ. Contour interval is 10 dBZ from 10 dBZ. Bottom: Differential reflectivity factor (Z_{DR}) in dB.

top height of this rainband was not clear, but deduced to be higher than 6 km. From the vertical pointing C-band radar, the rainband had echo top height of about 10 km (20dBZ threshold) when it passed over the radar site. The Doppler radar data at 0358JST as shown in Fig. 15 indicated that it was also 10 km in height. The vertical wind component of the rainband B was derived from MU radar (when the passage over the radar site) and Doppler radar RHI scan (at 0358JST). When the rainband passed over the radar site, the strong downdraft (>2 ms^{-1}) did not reach lower level (it existed from 3.0 km to 3.3 km in height), while the strong downdraft appeared at around 2 km in height when the rainband A passed over the radar site. The RHI scan data indicated that the downdraft existed below 1 km at 0358JST.

There are several differences between the rainband A and B: echo top height, propagation direction, and surface wind. In order to clarify the differences between them further, we examined the cloud physical characteris-

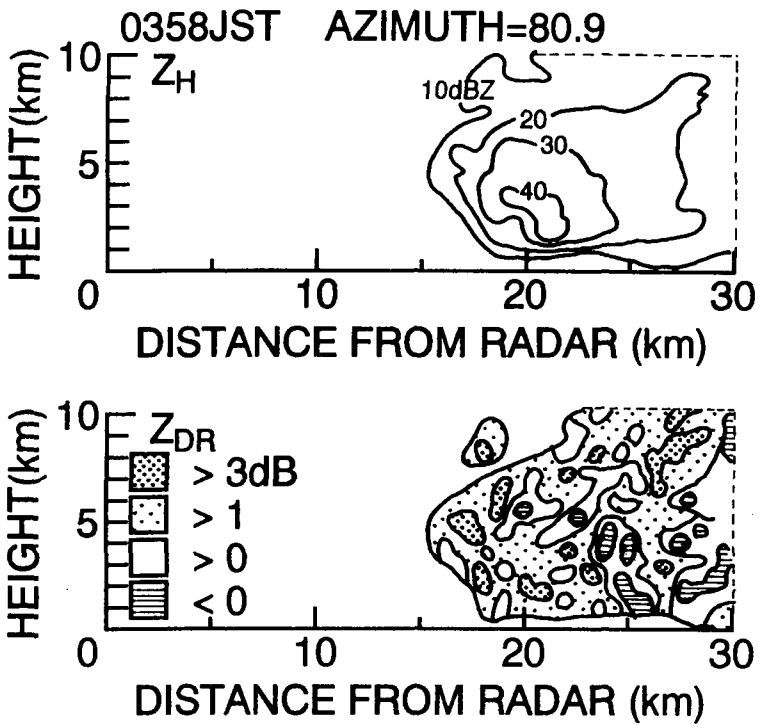

Fig. 15. Vertical cross section (RHI) of the rainband A at the azimuth of 80.9° at 0358JST on July 5, 1991. Top: Reflectivity (Z_H) in dBZ. Contour interval is 10 dBZ from 10 dBZ. Bottom: Differential reflectivity factor (Z_{DR}) in dB.

tics which is shown in the next section.

5. Cloud physical analysis

In this section, cloud physical processes of the rainbands are described from dual-polarization radar data and drop size distribution which was derived from the optical sensor placed at the MU radar site. As mentined in the Figs. 5 and 6, two rainbands passed over the radar site. Figure 16 shows the drop size distributions (DSD) of both rainbands (A and B). The DSD of the rainband A (left frame) is quite different from the rainband B when they passed over the radar site; larger drops were produced by the rainband A and recorded about 60 mmh^{-1} of rainfall intensity, on the other hand, smaller drops contributed for the strong rainfall intensity for rainband B. If we know DSD, horizontally polarized reflectivity factor Z_H and differential reflectivity factor Z_{DR} are

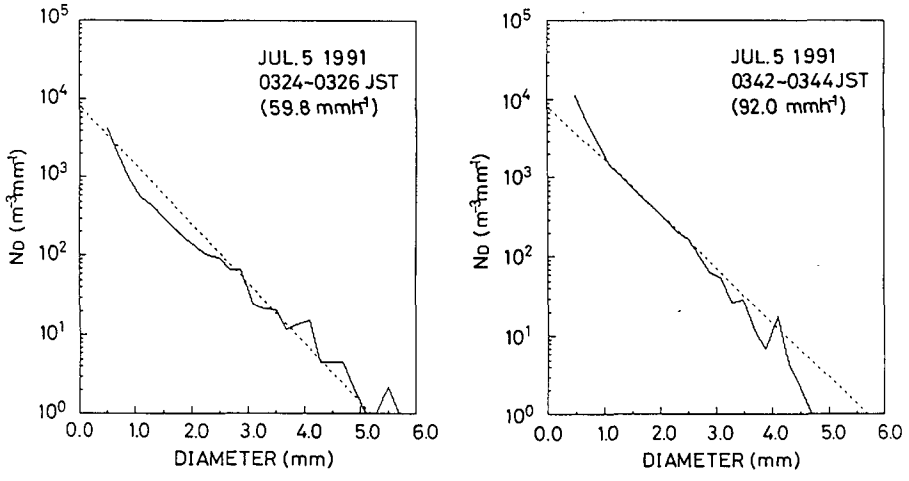

Fig. 16. Rain drop size distributions of the first rainband (left: 0324~0326JST on July 5, 1991) and the second rainband (right: 0342~0344JST).

calculated from the following procedure: horizontally and vertically polarized reflectivity factors, Z_H and Z_V are defined as,

$$Z_H=\int_0^\infty D^6\left|\frac{m^2-1}{4\pi+(m^2-1)P'}\right|^2 N(D)dD \tag{2}$$

$$Z_V=\int_0^\infty D^6\left|\frac{m^2-1}{4\pi+(m^2-1)P}\right|^2 N(D)dD \tag{3}$$

respectively, where D is rain drop diameter of equivalent volume, $N(D)$ is number concentration of drop size D, m is refractive index of water, and $P(P')$ is a kind of shape factor of rain drops. $P(P')$ is expressed as

$$P=\frac{4\pi}{e^2}\left[1-\left(\frac{1-e^2}{e^2}\right)^{\frac{1}{2}}\arcsin(e)\right] \tag{4}$$

$$P'=2\pi-P/2 \tag{5}$$

where e is eccentricity $e=\frac{(b^2-a^2)^{\frac{1}{2}}}{a}$ (a and b are short and long axis length, respectively).

The shape of a rain drop depends on its size; as the size increases the droplet becomes oblate (smaller droplets have a spherical shape). In this study the experimental relationship between the axis ratio and diameter of equivalent sphere is obtained by Pruppacher and Beard (1970);

$$a/b=[1-(9/16)a_0\rho V_t^2/S] \quad (140\ \mu m<a_0<500\ \mu m) \tag{6}$$

$$a/b=1.030-0.124a_0 \quad (500\ \mu m<a_0<4.5\ mm) \tag{7}$$

where a_0 is radius of the equivalent sphere, ρ is saturated air density, V_t is terminal fall velocity, and S is the surface tension of water of 20°C. Then differential reflectivity factor Z_{DR} is obtained from Eq. 1. A dual-polarization radar can derive Z_H, Z_V, and Z_{DR} values that are compared with the calculated values from DSD.

Table 2 shows the calculated value of Z_H and Z_{DR} of both rainbands from

Table 2. Calculated Z_H and Z_{DR} of two rainbands from DSD and Marshall- Palmer distributions of rainfall intensity.

Drop Size Distribution	Parameter	Rainband A (59.8 mm h^{-1})	Rainband B (92.0 mm h^{-1})
Observed	Z_{DR} (dB)	2.18	1.67
	Z_H (dBZ)	50.43	49.98
Marshall-Palmer	Z_{DR} (dB)	2.14	2.36
	Z_H (dBZ)	52.08	54.95

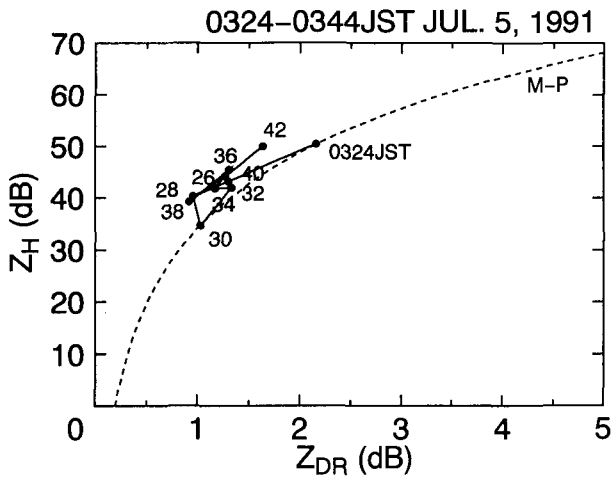

Fig. 17. Relationship of Z_H and Z_{DR} from 0342JST calculated from rain drop size distribution of surface observation. Dashed line expresses the relationship of Marshall-Palmer distribution (M-P).

observed DSD and Marshall-Palmer distribution of the same rainfall intensity. The rainband A (left column) shows Z_{DR} value close to that of Marshall-Palmer distribution, but the rainband B shows smaller Z_{DR} than that of Marshall-Palmer distribution, but the rainband B shows smaller Z_{DR} than that of Mar-

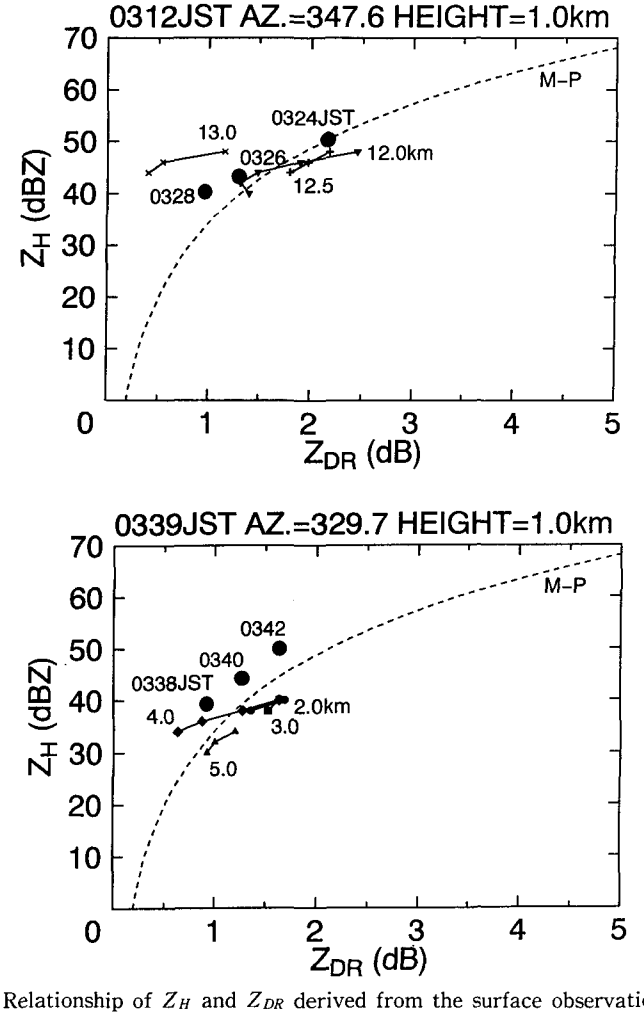

Fig. 18. Relationship of Z_H and Z_{DR} derived from the surface observation of rain drop size distribution (with time, same as Fig. 17 but expressed as large solid circles) and dual-polarization radar of 1 km in height (expressed symbols with line, and distances of the sampling area are noted). Top: 0312JST dual-polarization data and 0324JST to 0328JST surface data (first rainband). Bottom: 0339JST dual-polarization data and 0338JST to 0342JST surface data.

shall-Palmer distribution. During this observation, the DSD was derived from two minute intervals. Figure 17 expresses the transition of the relationship between Z_H and Z_{DR} from 0324JST to 0344JST (only this period was available). Figure 18 expresses a plot of Z_H and Z_{DR} from DSD and dual-polarization radar data of corresponding rainband. Both calculated and observed Z_H and Z_{DR}

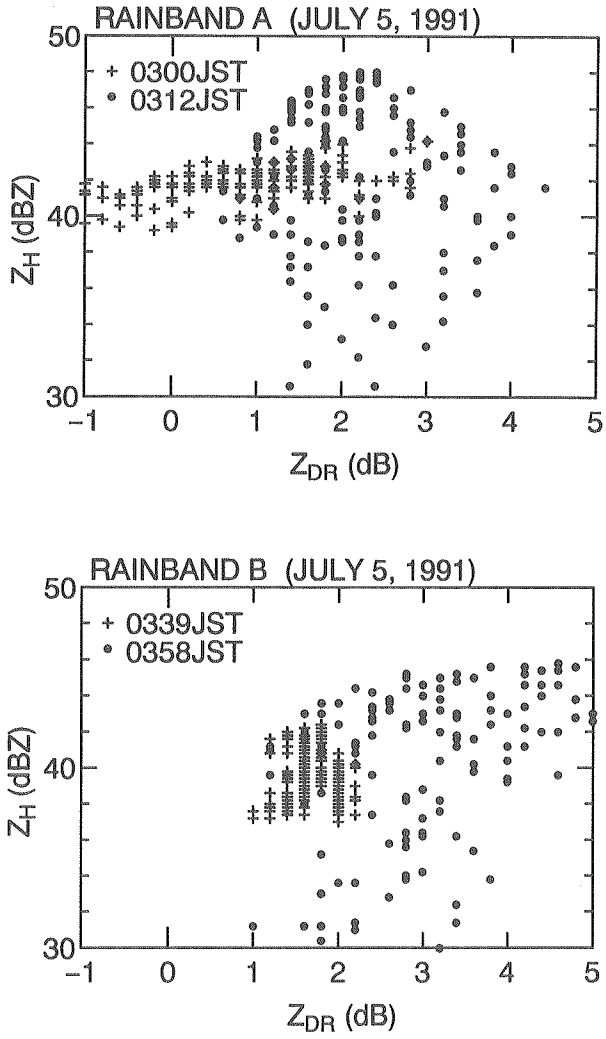

Fig. 19. Relationship between Z_H (>30 dBZ) and Z_{DR}, at the core region of developing and mature stages of rainband A (upper: at 0300JST and 0312JST) and B (bottom: at 0339JST and 0358JST).

show good agreement each other.

When we discuss the differences of the DSD between rainband A and B, we have to consider the differences of the stage during their life cycle. As shown in Figs. 9, 10, 14, and 15, the distribution of Z_{DR} value in the echo changed from the earlier stage to later stage. At the earlier stage, the relatively small Z_{DR} appeared in the strong echo region (>30 dBZ). On the other hand, the large Z_{DR} region appeared in the strong echo region at the later (mature) stage. As shown in Fig. 10 (rainband A), the downdraft occurred in the strong echo region at that time as same as the case in Fig. 15 (rainband B). The result is clearly expressed in Fig. 19. Figure 19 shows the relationship between Z_H and Z_{DR} at the core (strong reflectivity) region of both echoes at the earlier stage and mature stage shown in Figs. 9, 10, 14, and 15. Both frames in Fig. 19 indicate the relatively smaller Z_{DR} and variance of Z_{DR} at the earlier stage than mature stage.

As shown in the bottom frame of Fig. 10, the vertical structure of Z_{DR} of the first rainband had clearly large Z_{DR} at the strong reflectivity region. Also, it shows relatively low echo top height (around 6 km). This suggests that rainband A was consisted of warm rain at the leading edge. This case study suggests that warm rain process possibly exists in the Baiu season, and warm rain cloud and cold rain cloud coexisted in this case or warm rain process appeared in the early stage of life cycle of the rainband, same as the tropical cloud (Takahashi and Uyeda, 1995). The appearance of warm rain cloud is assumed to be caused by the stability of atmosphere; moist condition with neutral stability in the Baiu season might sometimes prevent the vertical development (in this case, stable layer existed at 6 km in height from Fig. 3) but has plenty of water vapor. On the other hand, once echo developed above the stable layer, cloud might develop rapidly because of the sensible heat release. This case study could not clarify how the diversity occurs, because this case study could not follow the life cycle of the rainband.

6. Comparison between rainband A and B

In sections 4 and 5, kinematic and cloud physical characteristics of rainbands A and B were explained. In this section, both rainbands will be compared from the viewpoints of existence of gust front, low level wind field, propagation direction and cloud physical characteristics, in order to specify the Baiu frontal rainbands.

At first, we summarize the stages when the rainbands passed over the radar site in their life cycle. The stage was determined from the in-cloud circulation

deduced from Doppler velocity field of RHI scan; when the echo was sustained by updraft, the echo was at the developing stage, and when the low level downdraft and upper level updraft coexisted, the echo was at the mature stage. From the analyses in section 4, when the rainband A passed over the radar site, the rainband was during its mature stage. On the other hand, when the rainband B passed over the radar site, the rainband was during its developing stage.

It is known as a common characteristic that the Z_{DR} values were small at the earlier stage and they became larger at the mature stage. On the other hand, differences are propagation direction and echo top height. On the echo top height, the rainband A showed that it was 10 km at earlier stage but was less than 6 km at the mature stage (echo top height was 5 km from vertical pointing C-band radar). It was related to the occurrence of convective outflow. On the other hand, the rainband B showed relatively higher echo top height (10 km from vertical pointing C-band radar when it passed over radar site and >10 km from X-band Doppler radar at the mature stage) through the life cycle. The propagation direction of the rainband A changed due to the initiation of gust front, while the propagation direction of the rainband B did not change through its life cycle from the JMA Osaka radar and Doppler radar analyses. These differences may be indicated that the rainband B did not produce a gust front, at least during the rainband existed within the observation area. In addition to above discussion, cold frontal characteristics were well expressed by the rainband A from the viewpoint of surface wind shift (SW to NW). When the rainband B passed over the radar site, the surface wind was also NW but weak. This result indicates that the different type of rainband generated in this case, even if the environmental condition was same.

7. Concluding remarks

In this study, Baiu frontal rainbands were analyzed by using dual-polarization Doppler radar, MU radar, and optical sensor for the drop size distribution from the viewpoint of meso-γ scale kinematics and cloud physical processes. Doppler radar analysis revealed that a rainband (rainband A) had echo top height of 6 km to 8 km through its life cycle, propagated to the east with 20 ms^{-1} of the propagation speed at the early stage and changed to the southeast with 12 ms^{-1} due to the occurrence of convective outflow. The rainband maintained its circulation by a gust front at the mature stage, and its formation process was dominated by shear instability that was similar to that of cold frontal rainband.

On the other hand, another rainband (rainband B), which generated behind

the rainband A, had different characteristics from the rainband A. It did not show the existence of gust front and kept relatively high echo top height of 10 km. The propagation direction was to the east with a speed of 20 ms^{-1} through its life cycle.

By calculating the differential reflectivity factor (Z_{DR}) from drop size distribution at the MU radar site, corresponding Z_{DR} value derived from dual-polarization radar was examined. The Z_{DR} values from dual-polarization data showed good agreement with the surface observation. Both rainbands showed relative small Z_{DR} values in their early stage, and the Z_{DR} values became larger at their mature stage. Cloud physical analysis and kinematic analysis on the rainband A indicate the coexistence of warm rain cloud and cold rain cloud because of the warm and moist condition of the Baiu season.

This case study clarified the influences of complex environment of the Baiu season on the Baiu frontal rainband ; midlatitudinal dynamic forcing contributed to the echo formation. On the other hand, thermodynamic condition showed subtropical. This suggestion on the characteristics of the Baiu frontal rainband is expected to be clarified by dynamic, thermodynamic and cloud physical observations in future.

Acknowledgments

The authors would like to express their thanks to Mr. Ishida, a student of the Meteorological Laboratory, Faculty of Science, Hokkaido University, for help the observation of radar and optical sensor. They also thank to Prof. S. Fukao, Radio Atmospheric Science Center, Kyoto University, and Prof. A. Sumi, Center for Climate System Research, University of Tokyo for their encouragement throughout the study. The authors extend their thanks to Drs. T. Tsuda, M. Yamamoto and T. Nakamura for their cooperation at the MU radar observatory, the Osaka District Meteorological Observatory kindly permitted to use the data of weather radar and weather data. The MU radar belongs to and is operated by the Radio Atmospheric Science Center of Kyoto University. This study was partly supported by the Grant-in-Aid for Scientific Research from the Ministry of Education, Science, and Culture of Japan (No. 06NP021).

References

Akiyama, T., 1973. Ageostrophic low-level jet stream in the Baiu season associated with heavy rainfall over the sea area. J. Meteor. Soc. Japan, **51**, 205-208.

Akiyama, T., 1978. Mesoscale pulsation of convective rain in medium-scale disturbances development in Baiu front. J. Meteor. Soc. Japan, **56**, 267-283.

Akiyama, T., 1984a. A medium-scale cloud cluster in a Baiu front. Part I: Evolution process and fine structure. J. Meteor. Soc. Japan, **62**, 485-504.

Akiyama, T., 1984b. A medium-scale cloud cluster in a Baiu front. Part II: Thermal and kinematic fields and heat budget. J. Meteor. Soc. Japan, **62**, 505-521.

Browning, K.A. and R. Wexler, 1968. The determination of kinematic properties of a wind field using Doppler radar. J. Appl. Meteor., **7**, 105-113.

Fukao, S., M.D. Yamanaka, T. Sato, T. Tsuda, and S. Kato, 1988. Three-dimensional air motion over the Baiu front observed by a VHF-band Doppler radar: A case study. Mon. Wea. Rev., **116**, 281-292.

Hobbs, P.V. and P.O. Persson, 1982. The mesoscale and microscale structure and organization of clouds and precipitation in midlatitude cyclones. Part V: The substructure of narrow cold-frontal rainbands. J. Atmos. Sci., **39**, 280-295.

Lemaitre, Y. and P. Brovelli, 1990. Role of a low level jet in triggering and organizing moist convection in a baroclinic atmosphere. A case study: 18 May 1984. J. Atmos. Sci., **47**, 82-100.

Lin, Y.-J., R.W. Pasken, and H.-W. Chang, 1992. The structure of a subtropical prefrontal convective rainband. Part I: Mesoscale kinematic structure determined from dual-Doppler measurements. Mon. Wea. Rev., **120**, 1816-1836.

Ninomiya, K. and T. Akiyama, 1972. Medium-scale echo clusters in the Baiu front as revealed by multi-radar echo maps. (Part I). J. Meteor. Soc. Japan, **50**, 558-569.

Ninomiya, K. and T. Akiyama, 1973. Medium-scale echo clusters in the Baiu front as revealed by multi-radar echo maps. (Part II). J. Meteor. Soc. Japan, **51**, 108-118.

Ogura, Y., T. Asai and K. Dohi, 1985. A case study of a heavy precipitation event along the Baiu front in northern Kyushu, 23 July 1982: Nagasaki heavy rainfall. J. Meteor. Soc. Japan, **63**, 883-900.

Pruppacher, H.R. and J.D. Beard, 1970. Microphysics of clouds and precipitation. D. Reidel Publishing Company, 714 pp.

Ray, P.S., A. Robinson and Y. Lin, 1991. Radar analysis of a TAMEX frontal system. Mon. Wea. Rev., **119**, 2519-2539.

Shimizu, S., H. Uyeda, R. Shirooka, A. Watanabe, A. Sumi and S. Fukao, 1992. Vertical structure of the Baiu front analyzed with the MU radar and an X-band Doppler radar. 11th Intn'l Conf. on Cloud and Precipitation, Montreal, 593-596.

Takahashi, N., 1994. Studies of the mesoscale and microscale features of heavy rainfall events during the late period of the Baiu season. Doctor thesis of Hokkaido University, 222 pp.

Takahashi, N. and H. Uyeda, 1995. Doppler radar observation on the structure and characteristics of tropical clouds during TOGA-COARE IOP in Manus, Papua New Guinea —Fundamental characteristics of tropical clouds through three case studies on November 23 and December 16, 1992—. J. Meteor. Soc. Japan, **71** (submitted).

Tao, W.-K. and J. Simpson, 1989. A further study of cumulus interactions and mergers: Three-dimensional simulations with trajectory analyses. J. Atmos. Sci., **46**, 2974-3004.

Uyeda, H. and D.S. Zrnić, 1986. Automatic detection of gust fronts. J. Atmos. Oceanic Technol., **3**, 36-50.

Westcott, N.E. and P.C. Kennedy, 1989. Cell development and merger in as Illinois thunderstorm observed by Doppler radar. J. Atmos. Sci., **46**, 117-131.